JOURNAL OF MATERIALS SCIENCE 23 (1988) 2824–2836

Theoretical study of the defect distribution of trivalent cation impurities in MgO

J. C. G. CARROLL, J. CORISH
Department of Chemistry, Trinity College, Dublin 2, Ireland

B. HENDERSON
The Department of Physics, University of Strathclyde, Glasgow G4 ONG, UK

W. C. MACKRODT
ICI plc, New Science Group, The Heath, Runcorn, Cheshire WA7 4QE, UK

Atomistic simulation techniques have been used to calculate defect energies for a range of trivalent cation impurities in MgO single crystals. From these, values of the association energies have been estimated for impurity–vacancy aggregates ranging in size from simple impurity–vacancy monomers, containing one impurity ion, to large clusters containing up to 24 impurity ions. For the $MgO:Cr^{3+}$ system, these energies have been incorporated in a mass-action analysis and predictions made of the dependence of the equilibrium distribution of defects on temperature and on the nominal concentration of the dopant.

1. Introduction

Many of the properties of MgO single crystals are determined by the presence of impurity ions, particularly aliovalent ions, whether these ions are introduced deliberately or are adventitiously present. The case of trivalent cations, present as substitutional impurities in MgO has been widely studied, both experimentally and theoretically. Interest in these systems arises primarily because of the association of the impurity ions with the oppositely charged cation vacancies that are created to preserve charge neutrality within the crystal. Experimentally, much attention has focused on the spectroscopic properties of trivalent transition metal cations embedded in the MgO lattice, and on how these properties are affected by the presence of nearby cation vacancies which reduce the symmetry of the environment experienced by the transition metal ion [1, 2]. Such investigations have provided detailed information on the types of defects present and have greatly increased our understanding of these systems. However, little quantitative information on defect formation and association energies has emerged. Furthermore, techniques such as diffusion and conductivity measurements which provide most of the available experimental information on defect formation, migration and association in the alkali and silver halides [3] have proved less successful in the study of oxides. In addition to the experimental difficulties in working at the higher temperatures required, the impossibility of obtaining "pure" crystals for investigation has made interpretation of experimental results more difficult. Therefore, although a number of studies of the diffusion and conductivity of $MgO:M^{3+}$ systems have been reported, the interpretation of the Arrhenius energies that are measured is often ambiguous [4–6].

For these reasons, reliable theoretical values for defect association energies for the $MgO:M^{3+}$ systems are desirable to allow prediction of the configurations of the impurity–vacancy associates that may form as an aid in the interpretation of experimental data. Following the success of atomistic simulation studies in calculating many of the experimentally measured defect parameters for the alkali and silver halides [7, 8], and the alkaline earth fluorites [9, 10], these techniques have also been used to study trivalent cation impurities in MgO [11, 12]. However, in these earlier calculations, both the range of trivalent cations and the configurations of impurity–vacancy aggregates considered have been rather limited. In this paper, calculated association energies are reported for sixteen trivalent cation impurities in MgO and the effect of impurity ion size is elucidated. A wide range of possible impurity–vacancy configurations is considered and the formation of large clusters is also investigated. Where possible, comparisons are made with experimental data. For Cr^{3+} we have examined the effect of temperature on the association energies of these clusters by considering the lattice expansion of the host crystal. Finally the results are incorporated in a mass action analysis of the $MgO:Cr^{3+}$ system which enables predictions to be made as to the equilibrium distribution of defects as a function of the concentration of impurity present and of the temperature.

2. Theoretical methods

The defect energies were calculated using the HADES suite of programs [13]. Such calculations have two main aspects: the representation of the lattice and the specification of appropriate interionic potentials to describe the short-range interactions between the ions. Both aspects have been described extensively

0022–2461/88 $03.00 + .12

TABLE I Energies of solution, in eV per impurity ion, for four possible solution processes. These were calculated using the potentials developed by Lewis [16] (see text)

Solution process	Impurity ion				
	V^{3+}	Fe^{3+}	Mn^{3+}	Ti^{3+}	Sc^{3+}
$M_2O_3(S) \xrightarrow{MgO} 2M_{Mg}^{\cdot} + V_{Mg}'' + 3O_0^x$	1.8	1.9	1.4	1.4	1.8
$M_2O_3(S) \xrightarrow{MgO} 2M_{Mg}^{\cdot} + O_i'' + 2O_0^x$	4.0	4.1	3.6	3.6	3.9
$M_2O_3(S) \xrightarrow{MgO} 2M_i^{\cdot\cdot\cdot} + 3V_{Mg}'' + 3O_0^x$	18.7	17.4	17.2	18.1	18.6
$M_2O_3(S) \xrightarrow{MgO} 2M_i^{\cdot\cdot\cdot} + 3O_i''$	25.3	24.0	23.8	24.7	25.2

elsewhere [14] and it is the quality of the interionic potential which primarily determines the reliability of calculated defect energies. In recent years, a number of potential models for MgO have been developed and two of these were used in the present study. The first, Potential I, was developed by Catlow *et al.* [15] using a semi-empirical fitting procedure in which the Mg^{2+} ion was treated as unpolarizable. The second, Potential II, was derived using the non-empirical electron gas methods of Mackrodt and Stewart [16] that incorporate the Madelung field of the crystal. The shell parameters of the O^{2-} ions were then obtained empirically by fitting to dielectric data and the Mg^{2+} ion was again regarded as unpolarizable. Two other empirical potentials [17, 18] are available and test calculations carried out during the course of this work showed them to be similar to Potential I. We shall therefore present results only for Potentials I and II with the exception of our calculations of the heats of solution of a number of trivalent ions in MgO (Table I) which were obtained using the potential developed by Lewis (his Potential B) [18]. These potentials alone provided the lattice energies for the M_2O_3 salts which are necessary for a self-consistent calculation of the heats of solution. In calculating the defect energies of impurity ions in a host crystal, it is important that the impurity ion–host ion potentials are derived by a method consistent with that used to derive the host crystal potential. This is easily achieved for electron gas potentials and the details of such potentials for a range of trivalent cation impurities in MgO are available in the compilation of Colbourn *et al.* [19] which also includes the details of Potential II. The potentials are numerical in form and the program evaluates them, and their first and second derivatives which are necessary for the energy minimization, using cubic splining routines which were incorporated for this purpose. With Potential I, the impurity ion–host ion parameters used were those obtained from the potentials for M_2O_3 type oxides derived by Lewis [18]. These semi-empirical potentials are in the Buckingham or Born–Mayer form which is more usual in simulations of this type. The results of calculations using the two potentials make it possible to compare their suitability to represent the systems under study.

3. Calculated defect energies

3.1. Small aggregates

The intrinsic defect energies and crystal properties calculated using these two MgO potentials have been reported elsewhere [12, 15]. In each case, agreement with available experimental values is reasonable. Both experimental and theoretical investigations indicate that in MgO doped with trivalent cations, the predominant defects are substitutional impurities with extrinsic cation vacancies being created to preserve charge neutrality: two substitutional ions for each cation vacancy. Table I shows heats of solution calculated using the MgO Potential B developed by Lewis [18] for five trivalent cations in MgO for four possible solution processes. The process involving the formation of substitutional impurities with charge compensating cation vacancies is found to have the lowest energy and is, therefore, clearly predicted to be that most likely to occur. In the Kroger–Vink notation [20], which is used in this paper, these defects are denoted as $M_{Mg}^{\cdot}$ and V_{Mg}'', respectively. The heats of solution given in Table I assume that the $M_{Mg}^{\cdot}$ and V_{Mg}'' defects exist as isolated species in the lattice. These species do, however, carry opposite virtual charges and it is likely, therefore, particularly when they are present at higher concentrations, that they will associate to form impurity–vacancy monomers, dimers and eventually larger clusters. The simplest complex which may form is one containing a single impurity ion and a single cation vacancy. These species, referred to here as monomers, are not charge neutral: their net charge is -1. Local charge compensation is fully achieved when a second impurity ion joins the monomer thus forming a dimer. (It should be noted that in the literature pertaining to trivalently doped MgO, these two types of impurity–vacancy defects, referred to as monomers and dimers here, are often named as dimers and trimers, respectively. Clearly these designations may lead to confusion and the naming system adopted here is chosen because it is consistent with the system used to describe aggregates in the alkali halide and fluorite crystals [10, 21], where the prefixes mono-, di- and tri- refer to the number of impurity ions present in the aggregate rather than the total number of species which it contains.)

The first nearest-neighbour (nn) and second nearest-neighbour (nnn) impurity–vacancy monomer configurations are shown in Fig. 1. Their association energies ($\Delta u_{monomer}$) were evaluated as

$$\Delta u_{monomer} = u[(M_{Mg}V_{Mg})'] - u(V_{Mg}'') - u(M_{Mg}^{\cdot}) \quad (1)$$

The calculations use the two-region strategy in which the forces between the ions immediately surrounding the defect, Region I, are treated explicitly whereas the more distant ions, Region II, are computed in the harmonic approximation. The sizes of Region I used for all of the defect configurations were carefully

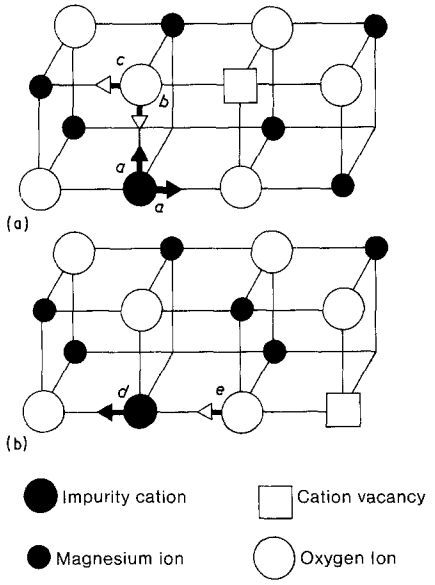

Figure 1 Structures of (a) nn and (b) nnn impurity vacancy monomers. The arrows indicate the direction of ionic displacements and the magnitudes of these displacements are given in Table II.

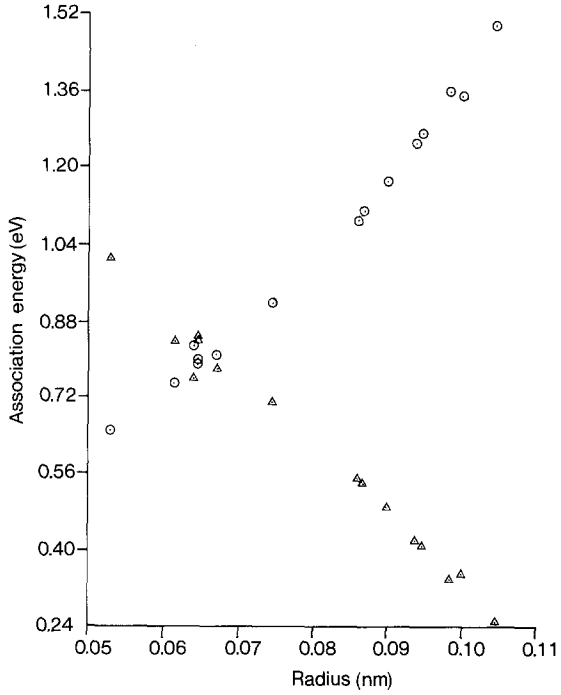

Figure 2 The dependence of the association energies for (○) nn and (△) nnn $(M_{Mg}V_{Mg})'$ monomers, calculated using Potential I, on the effective ionic radii of the impurity ions.

matched and were chosen to contain sufficient ions to ensure convergence. The numbers of ions in Region I for nn and nnn monomers, were 167 and 170, respectively. Because of problems with excessive core–shell separations in some calculations, all impurity ions were treated as unpolarizable. The results are presented in Table II and the variations in the association energies calculated with Potential I with dopant ion size is shown in Fig. 2. The displacements of surrounding ions are also given. The relative stabilities of the nn and nnn monomers are found to depend strongly on dopant ion size. For the nn monomer, there is an approximately linear increase in the

TABLE II The calculated association energies Δu_{nn} and Δu_{nnn}, in units of eV, and ionic displacements, in units of Mg–O lattice separation, for nn and nnn $(M_{Mg}V_{Mg})'$ monomers. The directions of the ionic displacements *a*, *b*, *c*, *d* and *e*, are defined in Fig. 1: positive values correspond to relaxation in the direction shown

(a) Potential I

M^{3+}	Δu_{nn}	*a*	*b*	*c*	Δu_{nnn}	*d*	*e*
Al^{3+}	0.65	0.025	0.100	0.070	1.01	0.012	0.154
Cr^{3+}	0.75	0.022	0.049	0.075	0.84	0.020	0.106
V^{3+}	0.83	0.026	0.027	0.078	0.76	0.021	0.086
Fe^{3+}	0.80	0.032	0.044	0.076	0.85	0.015	0.108
Mn^{3+}	0.79	0.028	0.044	0.076	0.84	0.017	0.106
Ti^{3+}	0.81	0.025	0.032	0.078	0.78	0.020	0.091
Sc^{3+}	0.92	0.035	0.009	0.082	0.71	0.018	0.073
Lu^{3+}	1.09	0.046	−0.031	0.090	0.55	0.018	0.034
Yb^{3+}	1.11	0.048	−0.035	0.091	0.54	0.018	0.030
Y^{3+}	1.17	0.052	−0.048	0.095	0.49	0.018	0.017
Ho^{3+}	1.17	0.052	−0.047	0.095	0.49	0.018	0.017
Gd^{3+}	1.25	0.058	−0.063	0.099	0.42	0.017	0.002
Eu^{3+}	1.27	0.059	−0.067	0.101	0.41	0.016	−0.003
Nd^{3+}	1.36	0.067	−0.083	0.106	0.34	0.015	−0.019
Pu^{3+}	1.35	0.065	−0.081	0.105	0.35	0.015	−0.016
La^{3+}	1.50	0.078	−0.107	0.114	0.25	0.013	−0.042

(b) Potential II

M^{3+}	Δu_{nn}	*a*	*b*	*c*	Δu_{nnn}	*d*	*e*
Al^{3+}	0.71	0.068	0.159	0.081	0.94	0.004	0.250
Ni^{3+}	0.86	0.030	0.053	0.107	0.66	0.021	0.153
Co^{3+}	0.86	0.030	0.053	0.107	0.65	0.021	0.153
Cr^{3+}	0.87	0.031	0.053	0.107	0.65	0.020	0.154
Ga^{3+}	0.85	0.029	0.055	0.107	0.66	0.021	0.153
Fe^{3+}	0.86	0.030	0.053	0.107	0.65	0.020	0.153
Mn^{3+}	0.87	0.030	0.053	0.107	0.65	0.020	0.154
Ti^{3+}	0.87	0.032	0.054	0.106	0.66	0.019	0.156
Sc^{3+}	0.87	0.032	0.055	0.106	0.66	0.019	0.157
In^{3+}	1.05	0.037	0.003	0.116	0.44	0.023	0.107
Y^{2+}	1.05	0.039	0.007	0.115	0.46	0.022	0.113

TABLE III Calculated association energies Δu_{nn} and Δu_{nnn}, in units of eV, for nn and nnn ($M_{Mg}Li_{Mg}$) complex using Potential II. Note: $u(Li'_{Mg}) = 16.24$ eV

M^{3+}	Δu_{nn}	Δu_{nnn}
Al^{3+}	0.37	0.50
Ni^{3+}	0.47	0.35
Co^{3+}	0.47	0.35
Cr^{3+}	0.47	0.34
Ga^{3+}	0.47	0.35
Fe^{3+}	0.47	0.34
Mn^{3+}	0.48	0.34
Ti^{3+}	0.47	0.35
Sc^{3+}	0.47	0.35
In^{3+}	0.56	0.25
Y^{3+}	0.56	0.26

magnitude of the association energy with the increase in the size of the impurity ion, whereas for the nnn monomer, the opposite trend is observed. The systems considered here show that, in general, for impurity ions which are smaller than the host cation, the nnn monomer is more strongly bound, whereas for impurity ions larger than the host cation, the nn monomer becomes the more strongly bound of the two. Both experimental and computer simulation results for the alkali halides find an analogous behaviour as do previous calculations for MgO [12] and this is explained in terms of the relaxation of the surrounding anions.

An alternative source of charge compensation in $MgO:M^{3+}$ systems is provided by monopositive ions such as Li^+, Na^+ and K^+ which are often present as substitutional impurities in MgO single crystals. As substitutional ions, M'_{Mg}, they have a single virtual negative charge and consequently may form neutral associates with $M^{\cdot}_{Mg}$ species. Calculations were carried out for one such monovalent ion, Li^+, and Table III lists the theoretical association energies for nn and nnn ($M_{Mg}Li_{Mg}$) complexes. These association energies, Δu, were calculated using the equation

$$\Delta u = u[(M_{Mg}Li_{Mg})] - u(M^{\cdot}_{Mg}) - u(Li'_{Mg}) \quad (2)$$

with Potential II only being used, because this alone provided a lithium ion–host ion potential, compatible with the set of impurity–host potentials [19]. Similar variations with dopant ion size were observed for these association energies as were evident for the $(M_{Mg}V_{Mg})'$ monomers. As the size of the trivalent impurity ion increases, the magnitude of the association energy for the nnn configuration decreases and that for the nn species increases. However, in all cases, the calculated association energy is approximately half that of the analogous $(M_{Mg}V_{Mg})'$ monomer, as might be anticipated from purely Coulombic considerations.

Returning to consider the impurity–vacancy monomers, the next step in their aggregation process involves the addition of a second trivalent impurity ion to form a neutral dimer. Consideration of only those structures in which the cation is in either an nn or nnn position to both impurity ions yields nine possible configurations. These structures, labelled A to I, are shown in Fig. 3. These same nine structures

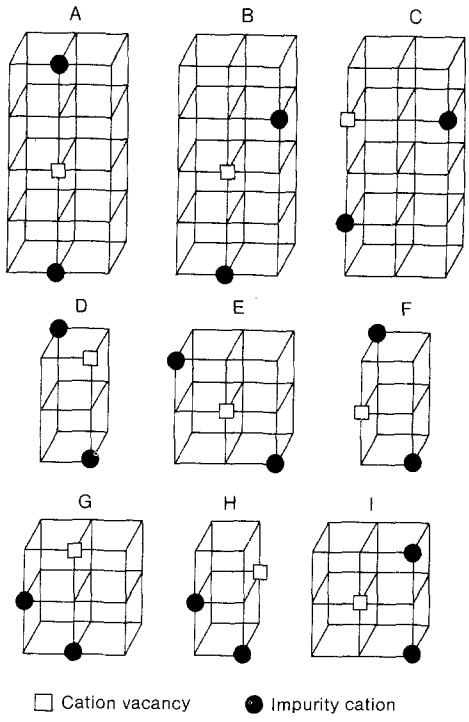

Figure 3 The structures of the nine ($M_{Mg}V_{Mg}M_{Mg}$) dimers for which association energies are reported in Table IV.

have been arrived at previously for the analogous case of impurity–divancy centres in alkali halides doped with divalent cations [22, 23]. The association energy of these dimers may be calculated either in terms of the total association energy of the dimer relative to its isolated constituents or in terms of the additional association energy which results when the second trivalent impurity ion is added to the monomer. The total association energies are given in Table IV and are calculated according to the equation

$$\Delta u^{tot}_{dimer} = u(M_{Mg}V_{Mg}M_{Mg}) - 2u(M^{\cdot}_{Mg}) - u(V''_{Mg}) \quad (3)$$

From this, the additional association energy may be calculated by subtracting the association energy of the appropriate monomer as given in Table II.

The variation of these association energies with dopant ion size is similar to that found for the monomers and occurs for the same reasons. The most stable dimer configuration changes from A to E and finally to F as the impurity ion size increases. The dimers in which both impurity ions are in nn positions to the vacancy, configurations E, F, H and I, show an increase in the magnitude of both the total and additional association energies with increasing dopant ion radius, whereas the opposite trend is observed for dimers A and C in which both impurities are in nnn positions to the vacancy. For those dimers (B, D and G) in which one impurity is in an nn position and the other in an nnn position relative to the vacancy, the total association energy is almost independent of the size of the impurity ion. However, the magnitude of the additional association energy increases with dopant ion radius when the second impurity ion adds on in an nn position whereas the opposite trend is observed when the second impurity

TABLE IV Calculated total association energies, Δu_x^{tot} (X ≡ A, B, . . . , I), in units of eV, for the dimers illustrated in Fig. 3

(a) Potential I

Mn^{3+}	A	B	C	D	E	F	G	H	I
Al^{3+}	1.87	1.11	1.72	1.45	1.03	1.08	1.25	0.96	0.62
Cr^{3+}	1.56	1.41	1.38	1.33	1.30	1.27	1.12	1.07	1.00
V^{3+}	1.41	1.42	1.25	1.32	1.46	1.41	1.09	1.15	1.24
Fe^{3+}	1.58	1.47	1.42	1.39	1.40	1.36	1.17	1.13	1.13
Mn^{3+}	1.57	1.45	1.40	1.37	1.37	1.34	1.15	1.12	1.10
Ti^{3+}	1.45	1.42	1.29	1.32	1.43	1.38	1.10	1.14	1.19
Sc^{3+}	1.30	1.45	1.14	1.34	1.64	1.59	1.09	1.26	1.47
Lu^{3+}	0.93	1.44	0.78	1.34	1.97	1.94	1.02	1.44	1.82
Yb^{3+}	0.89	1.44	0.75	1.34	2.01	1.98	1.04	1.47	1.86
Y^{3+}	0.75	1.43	0.62	1.35	2.12	2.11	1.03	1.54	1.94
Ho^{3+}	0.76	1.43	0.62	1.35	2.11	2.11	1.03	1.53	1.94
Gd^{3+}	0.58	1.42	0.45	1.37	2.26	2.29	1.02	1.63	2.04
Eu^{3+}	0.51	1.41	0.41	1.38	2.30	2.34	1.02	1.66	2.07
Nd^{3+}	0.35	1.40	0.23	1.41	2.45	2.54	1.02	1.77	2.14
Pu^{3+}	0.38	1.41	0.26	1.40	2.42	2.50	1.02	1.75	2.13
La^{3+}	0.07	1.38	−0.04	1.48	2.67	2.86	1.04	1.95	2.22

(b) Potential II

M^{3+}	A	B	C	D	E	F	G	H	I
Al^{3+}	1.75	1.43	1.61	1.42	1.15	1.17	1.20	0.99	0.75
Ni^{3+}	1.19	1.35	1.04	1.24	1.54	1.49	0.99	1.17	1.39
Co^{3+}	1.19	1.35	1.04	1.24	1.55	1.50	0.99	1.17	1.39
Cr^{3+}	1.19	1.36	1.04	1.25	1.56	1.51	1.00	1.18	1.41
Ga^{3+}	1.21	1.35	1.06	1.24	1.53	1.48	0.99	1.16	1.37
Fe^{3+}	1.19	1.35	1.04	1.24	1.55	1.50	0.99	1.18	1.40
Mn^{3+}	1.19	1.36	1.04	1.25	1.56	1.51	1.00	1.19	1.42
Ti^{3+}	1.20	1.36	1.05	1.25	1.56	1.51	1.00	1.18	1.41
Sc^{3+}	1.21	1.37	1.06	1.26	1.55	1.50	1.00	1.18	1.40
In^{3+}	1.68	1.28	0.55	1.20	1.89	1.88	0.88	1.37	1.76
Y^{3+}	0.72	1.30	0.57	1.21	1.89	1.87	0.88	1.37	1.74

ion adds on in an nnn position. For dimers in which the impurity ions are either both nn or both nnn to the vacancy, the magnitude of the additional association energy is less than the magnitude of the association energy of the corresponding monomer. This effect increases with the size of the impurity ion. It also becomes more pronounced as the separations of these species in the various configurations is decreased this is due primarily to the Coulombic forces between them.

If we refer to dimers as homogeneous when both of the impurity ions are the same, it is clear that a large number of heterogeneous dimers, involving two different trivalent impurity ions can be formed. We have carried out a limited number of calculations on such systems and these show, in general, that the total association energies are an average of the total association energies calculated for the two corresponding homogeneous dimers.

Neutral complexes may also form by association of dimers to form tetramers and larger aggregates. Although there are many possible combinations of two dimers, only one tetrameric structure is considered here. This is shown in Fig. 4 and is formed from two dimer B complexes. The calculated association energies for the formation of this tetramer from its isolated constituents and also from two B type dimers are listed in Table V and show a decrease in the magnitude of the association energy with increasing dopant ion size. For ions smaller than Sc^{3+}, this tetramer is bound relative to two dimer B complexes whereas this is not the case for larger ions. This is presumably due to the elastic strain involved in putting large dopant ions close together. Thus, for small dopant ions, the formation of tetramers from dimers is possible, although the net energy gain in this case is rather small.

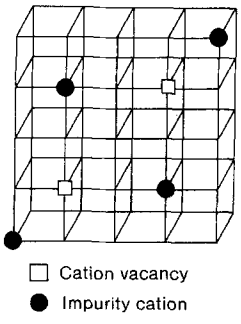

Figure 4 The structure of the tetramer for which association energies are reported in Table V.

3.2. Large aggregates

Quantitative experimental investigations of Cr^{3+} ions in MgO have indicated that the amount of impurity ions detected as isolated ions and in the form of simple monomeric and dimeric species is considerably less than the analytical chromium concentration [24]. This observation may be interpreted as evidence for the existence of significant concentrations of larger clusters of Cr^{3+} ions. Because such clusters have not yet been identified experimentally, suggestions as to their

TABLE V Calculated association energies, in eV per vacancy, for the tetramer shown in Fig. 4

M^{3+}	Relative to isolated defects		Relative to dimer B defects	
	Potential I	Potential II	Potential I	Potential II
Al^{3+}	1.84	1.79	0.73	0.36
Ni^{3+}	*	1.44	*	0.09
Co^{3+}	*	1.44	*	0.09
Cr^{3+}	1.66	1.44	0.25	0.08
Ga^{3+}	*	1.44	*	0.09
V^{3+}	1.59	*	0.17	*
Fe^{3+}	1.71	1.44	0.24	0.09
Mn^{3+}	1.68	1.44	0.23	0.08
Ti^{3+}	1.61	1.45	0.19	0.09
Sc^{3+}	1.56	1.46	0.11	0.09
In^{3+}	*	1.13	*	−0.17
Lu^{3+}	1.38	*	−0.06	*
Yb^{3+}	1.36	*	−0.06	*
Y^{3+}	1.29	1.17	−0.14	−0.13
Ho^{3+}	1.29	*	−0.14	*
Gd^{3+}	1.21	*	−0.21	*
Eu^{3+}	1.18	*	−0.23	*
Nd^{2+}	1.09	*	−0.31	*
Pu^{3+}	1.11	*	−0.29	*
La^{3+}	0.96	*	−0.42	*

*The impurity ion is not included in this potential set.

structure must be speculative. Gourdin and Kingery [11] proposed the existence of spinel-like impurity–vacancy aggregates in these systems, similar to the type of structure investigated theoretically by Catlow and Fender [25] in $Fe_{1-x}O$ crystals. These aggregates all contain a basic structural unit consisting of a tetrahedrally coordinated interstitial cation surrounded by four cation vacancies, with trivalent impurities symmetrically distributed around this tetrahedron to reduce the overall charge of the cluster. This basic unit is referred to as the 4–1 cluster. The interstitial cation may be either a host or an impurity cation. Further aggregations of these 4–1 clusters is possible, leading ultimately to spinel-type structures and this may occur either by edge sharing or corner sharing of the basic tetrahedral unit. X-ray, neutron and electron diffraction and electron microscopic studies in $Fe_{1-x}O$ have led to a number of proposals for the type of clusters present, based on the 4–1 unit. Calculated association energies are reported here for selected aggregates, namely the 4–1, 6–2, 8–2, 16–5, 24–5 and 24–5-a clusters, originally proposed by Gourdin and Kingery [11], where the numbers refer to the numbers of substitutional and interstitial ions, respectively. The structures of these complexes are shown in Fig. 5. The first three of these, the 4–1, 6–2 and 8–2 clusters, may contain either Mg^{2+} ions or trivalent impurity ions as interstitials, without making the overall charge on the defect excessively high. The notation used by Gourdin and Kingery for these three structures is augmented, where necessary, by an additional term in brackets indicating whether the interstitial ions in the cluster are trivalent dopant ions (M^{3+}) or host cations (Mg^{2+}). The 16–5 cluster, a corner-sharing arrangement of five tetrahedral units, models a portion of an inverse spinel structure whereas the 24–5 cluster, also corner sharing, forms the basis of the normal spinel structure. The 24–5-a cluster differs from the 24–5 only in the arrangement of the compensating trivalent substitutional ions surrounding the basic tetrahedral units. Similarly, the 8–2 cluster differs from the 6–2 cluster only in the number and arrangement of the charge-compensating substitutional impurities surrounding the defect.

In calculating the association energies of these

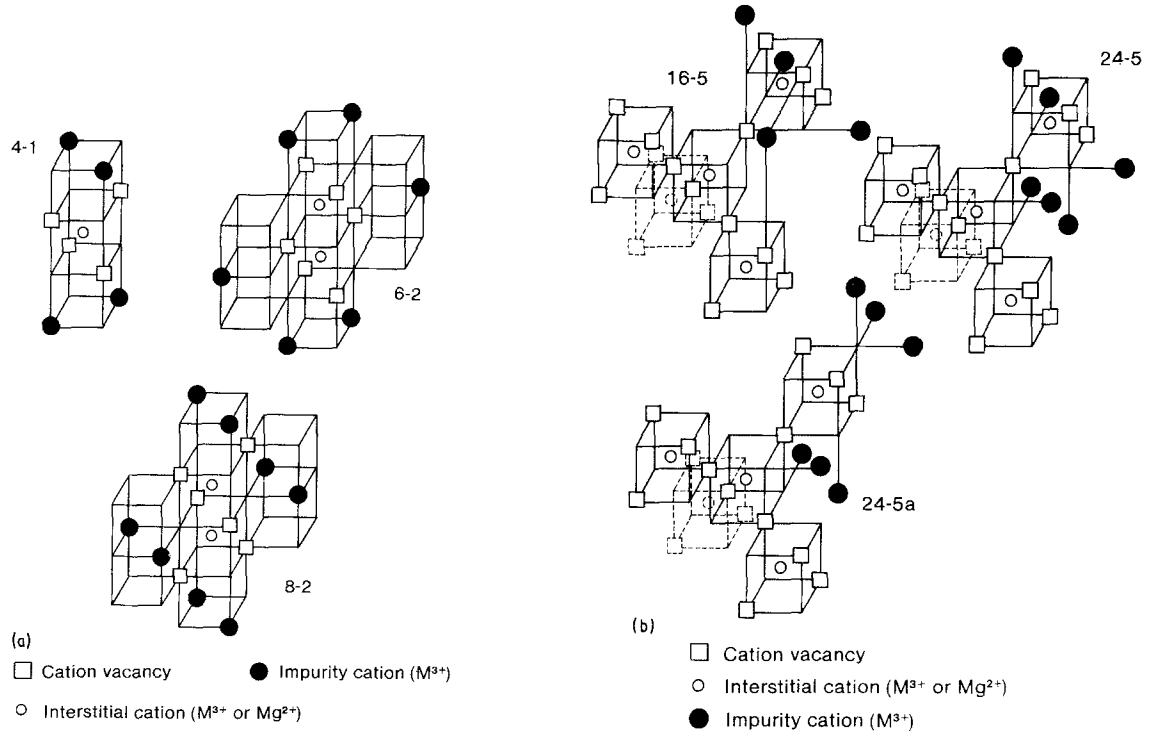

Figure 5 Structures of the larger clusters: (a) edge-sharing clusters; (b) corner-sharing clusters with the positions of the substitutional trivalent impurity cations shown for only one of the four tetrahedral units about the central tetrahedron: the remaining substitutional impurities occupy symmetrically equivalent positions about each of the other three tetrahedral units.

TABLE VI The numbers of defect species and the overall charges for the larger clusters: the notation used is explained in the text

	Cluster								
	4–1(M^{3+})	4–1(Mg^{2+})	6–2(M^{3+})	6–2(Mg^{2+})	8–2(M^{3+})	8–2(Mg^{2+})	16–5	24–5	24–5-a
Total V''_{Mg}	4	4	6	6	6	6	16	16	16
Total $M^{\cdot}_{Mg}$	4	4	6	6	8	8	16	24	24
Total $M_i^{\cdot\cdot\cdot}$	1	0	2	0	2	0	5	0	0
Total $Mg_{gi}^{\cdot\cdot}$	0	1	0	2	0	2	0	5	5
Net V''_{Mg}	3	3	4	4	4	4	11	11	11
Net $M^{\cdot}_{Mg}$	5	4	8	6	10	8	21	24	24
Net charge	−1	−2	0	−2	2	0	−1	2	2

clusters, the isolated constituents are taken to be in their most stable positions. For the systems considered here, this requires that each trivalent interstitial ion, in association with a cation vacancy, be treated as arising from the migration of a trivalent substitutional ion to an interstitial site. Similarly each interstitial magnesium ion, in association with a cation vacancy, is treated as arising from a normal lattice site. In this way, the defect energies of the isolated constituents are calculated in terms of net vacancies and net substitutionals, with the net number of interstitials being zero. Table VI shows both the total and net number of vacancies, substitutional ions and interstitial ions present in each cluster, together with its overall charge. The association energies of these complexes were calculated using the equation

$$\Delta u_{\text{cluster}} = u(\text{cluster}) - Vu(V''_{Mg}) - Su(M^{\cdot}_{Mg}) \quad (4)$$

where V is the net number of vacancies and S is the net number of substitutional ions. Finally, so that comparisons with the calculated association energies of monomeric and dimeric complexes are valid, the association energies of these clusters were calculated per net vacancy and the results are given in Table VII. Because of the large size of these clusters, these calculations were carried out using ~ 380 ions in Region I.

It is evident that clusters containing impurity interstitials are significantly more stable than the equivalent clusters involving host cation interstitials with the exception of the 8–2 clusters for which both configurations give similar association energies. These results suggest that the arrangement of the charge-compensating substitutional ions is a significant factor in determining the association energies of these complexes. With the exception of the larger dopant ions, there is a small increase in the magnitude of the calculated association energy per vacancy as the size of the cluster increases, although this increase is perhaps too

TABLE VII Calculated association energies, in units of eV per net vacancy, for the clusters shown in Fig. 5

(a) Potential I

M^{3+}	4–1*	4–1†	6–2*	6–2†	8–2*	8–2†	16–5	24–5	24–5-a
Al^{3+}	1.72	1.49	2.19	1.50	2.05	2.03	2.25	2.05	2.39
Cr^{3+}	1.89	1.48	1.99	1.43	2.03	2.08	2.20	2.18	2.43
V^{3+}	2.06	1.53	2.02	1.45	2.19	2.21	2.32	2.22	2.47
Fe^{3+}	2.12	1.58	2.28	1.51	2.39	2.23	2.53	2.26	2.52
Mn^{3+}	2.06	1.55	2.20	1.49	2.29	2.19	2.43	2.24	2.49
Ti^{3+}	2.03	1.52	2.03	1.45	2.17	2.18	2.31	2.22	2.47
Sc^{3+}	2.33	1.62	2.26	1.52	2.54	2.39	2.61	2.26	2.55
Lu^{3+}	2.62	1.72	2.42	1.61	2.83	2.67	2.78	2.17	2.59
Yb^{3+}	2.67	1.73	2.46	1.63	2.88	2.71	2.82	2.16	2.60
Y^{3+}	2.75	1.77	2.54	1.67	2.97	2.80	2.86	2.10	2.61
Ho^{3+}	2.75	1.77	2.53	1.67	2.96	2.80	2.85	2.10	2.61
Gd^{3+}	2.88	1.83	2.68	1.75	3.11	2.94	2.93	2.03	2.64
Eu^{3+}	2.91	1.85	2.71	1.78	3.13	2.98	2.94	2.00	2.64
Nd^{3+}	3.03	1.91	2.88	1.88	3.26	3.12	3.00	1.91	2.66
Pu^{3+}	3.01	1.90	2.85	1.86	3.24	3.09	2.99	1.93	2.66
La^{3+}	3.21	2.03	3.18	2.06	3.45	3.33	3.07	1.76	2.69

(b) Potential II

M^{3+}	4–1*	4–1†	6–2*	6–2†	8–2*	8–2†	16–5	24–5	24–5-a
Al^{3+}	2.18	1.67	2.67	1.62	2.56	2.23	2.76	2.12	2.44
Ni^{3+}	2.25	1.61	2.09	1.58	2.33	2.39	2.46	2.19	2.51
Co^{3+}	2.36	1.61	2.10	1.58	2.34	2.40	2.46	2.19	2.51
Cr^{3+}	2.29	1.63	2.14	1.59	2.40	2.42	2.51	2.21	2.53
Ga^{3+}	2.23	1.60	2.07	1.57	2.31	2.38	2.44	2.19	2.50
Fe^{3+}	2.28	1.62	2.12	1.59	2.37	2.41	2.48	2.21	2.52
Mn^{3+}	2.29	1.63	2.13	1.60	2.39	2.42	2.50	2.21	2.53
Ti^{3+}	2.31	1.63	2.17	1.60	2.43	2.43	2.53	2.22	2.53
Sc^{3+}	2.30	1.63	2.18	1.60	2.42	2.42	2.53	2.22	2.53
In^{3+}	2.38	1.69	2.01	1.69	2.42	2.70	2.35	1.99	2.51
Y^{3+}	2.45	1.70	2.12	1.69	2.53	2.71	2.47	2.04	2.53

*The cluster contains M^{3+} interstitials.
†The cluster contains Mg_{2+} interstitials.

small to constitute evidence for the continuation of the aggregation process to yield the larger clusters. Comparing the association energies for the 24–5 and 24–5-a clusters, the large effect of the positions of the surrounding substitutional ions is again apparent and this is especially true for the larger impurity ions.

The magnitude of the association energy of the 4–1 (M^{3+}) cluster is considerably larger than that of any of the dimers considered. This is true for all impurity ions, with the exception of the value for Al^{3+} calculated using Potential I. This suggests that such clustering is generally thermodynamically favoured, at least in its initial stages.

3.3. Temperature effects

In practical considerations we are concerned principally with defect configurations and association energies in MgO that are relevant at high temperatures. For this reason we now calculate the changes which occur in these entities as the temperatures is increased. The principal effect of temperature is lattice expansion and for internal consistency this has been calculated using the method introduced by Allen *et al.* [26]. A minor point to be noted here is that the potentials we have used to calculate the lattice expansion, namely those developed by Catlow *et al.* [15], were based on zero mechanical strain for a lattice parameter of 0.2106 nm which is the value reported by Peckham [27] for MgO at 298 K. As zero mechanical strain corresponds to zero K of temperature for a classical lattice, these potentials contain a slight inconsistency. However, because we are concerned here with changes in the defect association energies that result from lattice expansion, i.e. Δu as a function of $\Delta a(T)$, and as we shall be considering a very extensive temperature range, this minor inconsistency is of no significance for the present results.

In the method of Allen *et al.* [26] for the calculation of the lattice expansion, the lattice parameter, a, and the temperature, T, are derived from the gradient, $[\delta u(a)/\delta s(a)]_T$, in which $u(a)$ and $s(a)$ are the energy and entropy, respectively, of the perfect lattice. The calculated temperature dependence of a, using Potential I, is shown in Fig. 6, from which we obtain values of the linear expansion coefficient, α, of $9.3 \times 10^{-6}\,K^{-1}$ from 0 to 1000 K and $10.6 \times 10^{-6}\,K^{-1}$ from 0 to 2000 K, compared with experimental values of 9 to $15 \times 10^{-6}\,K^{-1}$ in the temperature range 500 to 1700 K [28]. We have confined our attention of Potential I but note that differences in the lattice expansion based on potentials have been reported to be small [26].

With regard to some of the formalities associated with finite temperature calculations, it has been pointed out previously [29] that experimentally determined quantities almost invariably correspond to lattices at constant pressure, rather than at constant volume and that there are differences in the values of defect parameters calculated under these two conditions [26, 30]. In general, the defect enthalpy at constant pressure, h_p, is not equal to the internal energy at constant volume, u_v, although in many cases, h_p is nearly constant over a wide range of temperature with a value close to that of u_v at 0 K. This, of course, is the reason why there has so often been good agreement between experimentally determined and calculated defect energies. Typically, h_p and u_v for the formation of defects differ by 0.5 to 1.5 eV over a temperature range of 2500 K [26]. Differences between h_p and u_v for point defect association, on the other hand, differ by only a few tenths of an electron volt or less [31]. For the present, therefore, and largely for the purpose of illustrating the effects of elevated temperatures, we restrict our attention to the temperature dependence of defect association energies at constant volume and confine our examples to defect associates involving Cr^{+3} and to calculations based on Potential I.

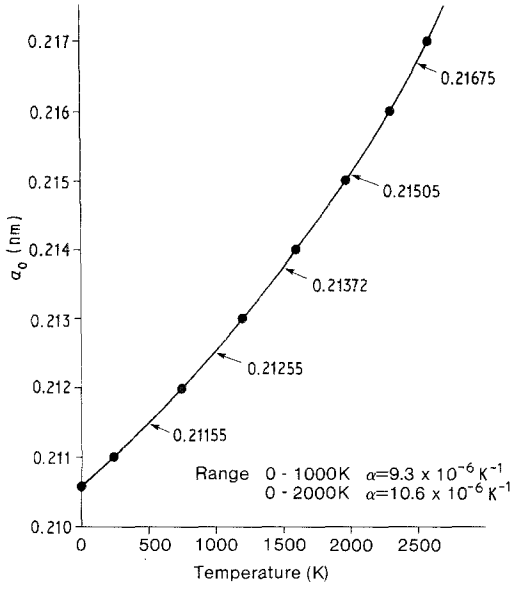

Figure 6 Calculated lattice expansion for MgO based on the interionic potential of Catlow *et al.* [15].

Reference to Table I indicates that at low temperature, substitutional impurity ions compensated by cation vacancies is the preferred, i.e. lowest energy mode of solution of M_2O_3 oxides in MgO, with oxygen interstitial compensation some 2.2 eV higher in energy. The first point we wish to consider, then, is whether or not the mode of solution of Cr^{3+}, and other trivalent impurities changes at elevated temperatures. The two remaining modes are at least 13 eV more energetic and hence unlikely to be of any significance up to the melting point of MgO. In the absence of defect association, the difference between the energies of solution for cation vacancy and oxygen interstitial compensation, Δu_s, is given per impurity ion by

$$\Delta u_s = \tfrac{1}{2}\,[u(O_i'') - u(V_{Mg}'') - u_L(MgO)] \quad (5)$$

in which $u_L(MgO)$ is the lattice energy of MgO and $u(O_i'')$ and $u(V_{Mg}'')$ are the defect energies of the interstitial oxygen and magnesium vacancy species, respectively. We note that as the substitution energies for the trivalent ion occurs in both modes of solution the results are valid for all trivalent ions. At low temperature, Δu_s is ~ 2.2 eV and hence cation vacancy compensation predominates: but does this remain the case at higher temperatures? Table VIII shows the temperature dependence of Δu_s for constant volume defect

TABLE VIII The difference in the energies of solution per impurity ion (Δu_s in eV) for two modes of solution involving impurity with anion interstitial compensation and cation vacancy compensation for $MgO:M^{3+}$ systems. The lattice parameters used in the calculation are shown and are based on the potential of Catlow *et al.* [15]. Δu (solution) is calculated using Equation 5

Temperature (K)	Lattice parameter (nm)	δu_s(eV)
0	0.210 60	2.20
500	0.211 55	2.06
1000	0.212 55	1.91
1500	0.213 72	1.75
2000	0.215 05	1.57
2500	0.216 75	1.34

energies based on Potential I. From this we see that while Δu_s certainly decreases with increasing temperature, vacancy compensation remains the predominant mode of solution even at the highest temperatures.

Turning now to defect association energies, Table IX shows calculated values of these as a function of temperature for the full range of associates from monomers to the 24–5-a complexes. As expected they decrease with increasing temperature/lattice parameter, by approximately 30% in the case of Cr^{3+} defects over the ~ 2500 K temperature range. The decreases in the individual association energies range from 0.33 eV for nnn monomers to 0.64 eV for the 4–1(M^{3+}) associates to 0.75 eV for the 24–5-a clusters. At elevated temperatures, therefore, the effect of lattice expansion is to destabilize the larger clusters relative to the smaller ones. Although a few changes in the order of stability of associates of the same size do occur the overall pattern remains essentially unchanged: nnn monomers remain more stable than nn monomers; A-type dimers remain the most stable and I-type the least stable of their size; 4–1(M^{3+}) associates remain more stable than 4–1(Mg^{2+}) and so on. Thus calculations would indicate that the overall degree of association decreases with temperature and that the distribution of associated Cr^{3+} impurity changes in favour of the smaller associates: we shall return to this effect in Section 4.

The final point we wish to consider here concerns such comparisons as can be made with experiment and, in particular, whether the calculated temperature dependence can be verified. Almost invariably, association energies cannot be measured directly, but are obtained from related quantities. What is clearly important, therefore, is the functional form of this relationship and the way in which the association energy is extracted. To illustrate this, we consider the formation of monomers, $(X_{Mg}V_{Mg})'$, from $X_{Mg}^{\cdot}$ and V_{Mg}''

$$X_{Mg}^{\cdot} + V_{Mg}'' \rightarrow (X_{Mg}V_{Mg})' \quad (6)$$

for which the association constant, λ, is given by

$$\lambda = [(X_{Mg}V_{Mg})']/([X_{Mg}^{\cdot}][V_{Mg}'']) \quad (7)$$

In the case of scandium impurity, Sempolinski and Kingery [6] have obtained λ as a function of temperature

$$\lambda = \lambda(T) \quad (8)$$

from which they have derived an association energy, u, of 0.73 eV by writing $\lambda(T)$ in the form,

$$\lambda(T) = A \exp(-u/kT) \quad (9)$$

In this case it is clear that u is to be identified with the association energy at 0 K and not at a high temperature value because if we write $\lambda(T)$ in the form

$$\lambda(T) = A' \exp[-u(T)/kT] \quad (10)$$

and assume a linear relationship so that

$$u(T) = u^0 - \Delta uT \quad (11)$$

then

$$\lambda(T) = A' \exp(\Delta u/k) \exp(-u^0/kT) \quad (12)$$

$$= A \exp(-u^0/kT) \quad (13)$$

TABLE IX Calculated defect association energies, in eV per vacancy, as a function of temperature for the range of defects considered. The lattice expansion is the same as that given in Table VIII

Defect	Temperature (K)					
	0	500	1000	1500	2000	2500
nn monomer	0.75	0.70	0.64	0.58	0.51	0.42
nnn monomer	0.84	0.80	0.77	0.73	0.68	0.62
Dimer A	1.56	1.51	1.44	1.37	1.28	1.17
Dimer B	1.41	1.33	1.25	1.15	1.05	0.91
Dimer C	1.38	1.35	1.29	1.22	1.14	1.04
Dimer D	1.33	1.26	1.19	1.11	1.01	0.89
Dimer E	1.30	1.20	1.10	0.98	0.86	0.70
Dimer F	1.27	1.18	1.08	0.97	0.85	0.70
Dimer G	1.12	1.06	1.00	0.93	0.85	0.75
Dimer H	1.07	0.99	0.91	0.82	0.72	0.59
Dimer I	1.00	0.91	0.81	0.70	0.58	0.44
Tetramer	1.66	1.58	1.50	1.40	1.29	1.15
4–1(M^{3+})	1.89	1.79	1.69	1.56	1.43	1.25
4–1(Mg^{2+})	1.48	1.43	1.37	1.29	1.21	1.10
6–2(M^{3+})	1.99	1.92	1.80	1.69	1.56	1.39
6–2(Mg^{2+})	1.43	1.38	1.33	1.27	1.19	1.09
8–2(M^{3+})	2.03	1.92	1.80	1.66	1.51	1.32
8–2(Mg^{2+})	2.08	1.98	1.88	1.75	1.61	1.44
16–5	2.20	2.09	1.98	1.84	1.68	1.47
24–5	2.18	2.07	1.95	1.81	1.65	1.44
24–5-a	2.43	2.32	2.20	2.06	1.89	1.68

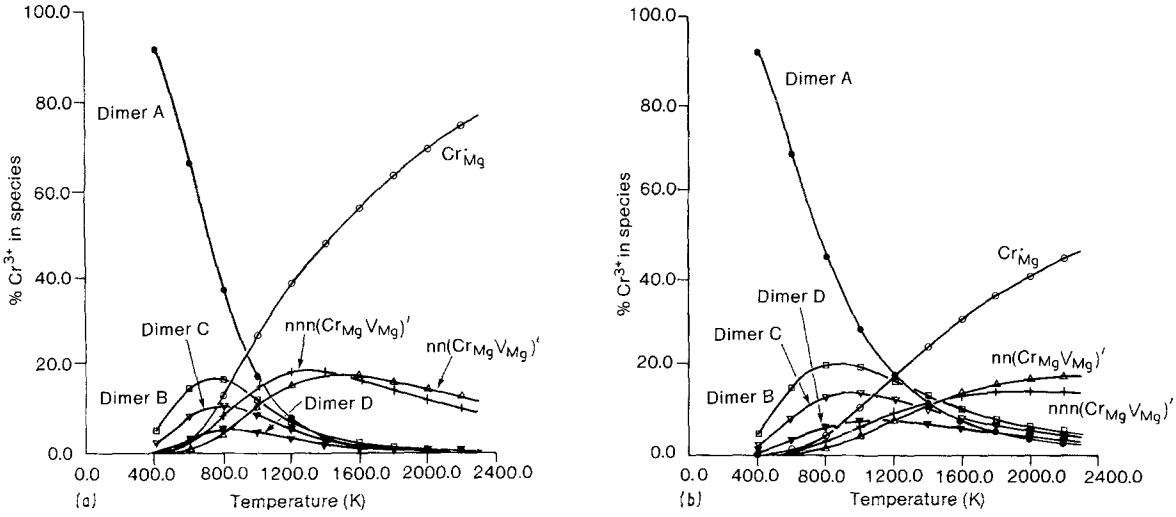

Figure 7 The equilibrium defect distribution of Cr^{3+} in MgO as a function of temperature when the mass-action analysis is restricted to monomeric and dimeric defects. In (a) the total Cr^{3+} concentration is 1000 p.p.m. and in (b) it is 10 000 p.p.m.: the analysis is based on association energies calculated using Potential I.

which is the form used by Sempolinski and Kingery [6]. It should be noted that our calculations confirm that such association energies are, in general, approximately linear functions of T at least up to 1500 K. To obtain the temperature dependence of the association energy, it would be necessary to know the value of A' independently. In general, therefore, the use of Arrhenius expression to extract energies, including migration energies, from experimentally determined temperature-dependent quantities, such as $\lambda(T)$, leads to values that are most appropriately compared with zero K calculations, rather than those relating to high temperatures.

4. Mass-action analysis

A useful way to assess the influence of the relative magnitudes of association energies of various defect complexes on the equilibrium defect distribution is to effect a mass-action analysis of the system. The relative stabilities of defect complexes with the same compositions is usually obvious from their association energies, but the relative stabilities of aggregates with different compositions are more difficult to assess. A full analysis of the relevant mass-action equations is required to reveal the equilibrium defect distribution. Such an analysis is based only on thermodynamic considerations and take no account of possible kinetic limitations.

The basic approach used in a mass-action analysis based on the results of atomistic simulation calculations has been described elsewhere [32]. In the results presented here, activity coefficients of unity have been assumed and non-configurational entropy terms are neglected. The case of Cr^{3+}, which is the most extensively studied trivalent impurity in MgO, is used to illustrate the general features of the defect equilibria in these systems.

Restricting the analysis initially to monomeric and dimeric aggregates and using the results from Potential I shown in Tables II, IV, V and VII, the defect equilibria at impurity concentrations of 1000 p.p.m. and 10 000 p.p.m. of Cr^{3+} are illustrated as a function of temperature in Fig. 7 in terms of the percentage of the total Cr^{3+} ions which occur in each aggregate. For clarity, only aggregates which contain 5% or more of the total impurity concentrations are included. These plots show a transition from a defect structure dominated by isolated impurities at high temperatures to one dominated by the most stable dimer (A) at low temperatures: the cross-over point occurs at higher temperatures in the more heavily doped crystals. The results indicate that at intermediate temperatures, there may be many different dimers present in significant amounts.

When all the larger aggregates for which association energies have been calculated are included in this type of analysis, then, as shown in Fig. 8, only two clusters, the 4–1(M^{3+}) and 24–5-a, are predicted to exist in significant quantities at lower temperatures. At the higher temperatures, these clusters have a negligible effect on the equilibrium distribution. As the temperature is lowered, however, the concentration of the 4–1(M^{3+}) cluster first rapidly increases and then decreases as the 24–5-a cluster begins to dominate. The majority of the impurity ions, at very low temperatures, are predicted to exist in this 24–5-a cluster. The temperature at which these two large clusters begin to appear in the defect equilibria increases with the total dopant concentration. It is interesting to note that the tetramer considered in these calculations is not predicted by the mass-action analysis to occur in significant quantities.

Clearly the mass-action approach depends critically on reliable values for the association energies of the complexes and on the assumption that all the complexes existing in the system have been included in the analysis. Nevertheless, it affords a reasonable guideline as to the response of the defect equilibrium to changes in temperature and in the concentration of the impurity.

We have also used the association energies calculated as a function of temperature and shown in Table IX in the mass-action programme to estimate the distribution of the impurity ion Cr^{3+}. The results at each of the temperatures varied very little from those shown in

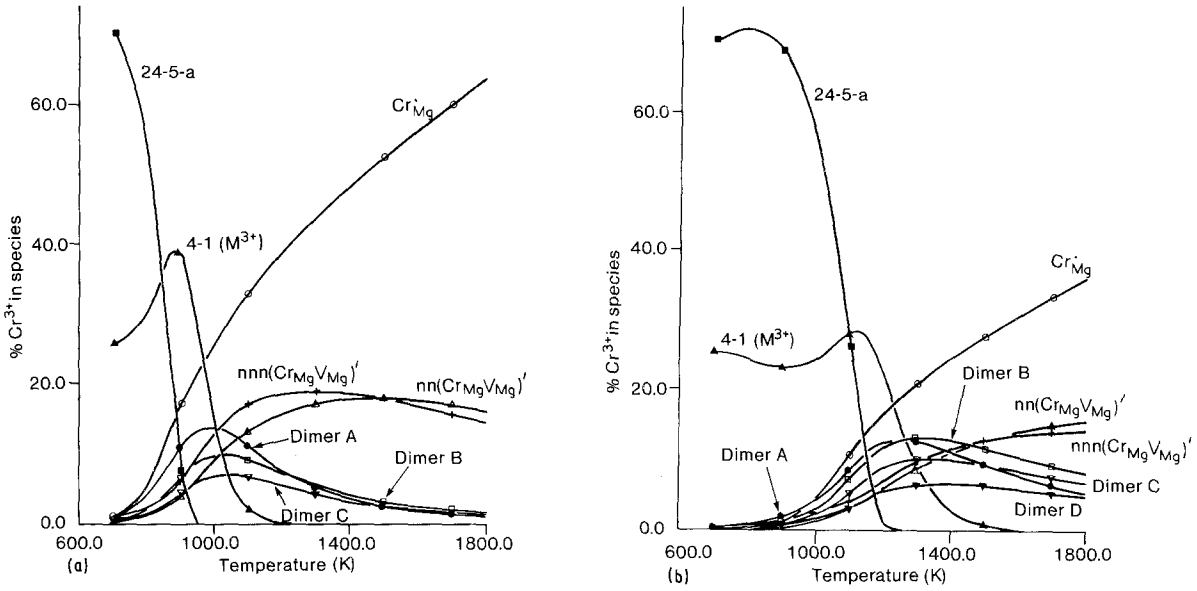

Figure 8 The equilibrium defect distribution of Cr^{3+} in MgO as a function of temperature when the mass-action analysis includes the larger clusters. In (a) the total Cr^{3+} concentration is 1000 p.p.m. and in (b) it is 10 000 p.p.m.: the analysis is based on association energies calculated using Potential I.

Figs 7 and 8 and in all cases no changes were found in the principal features of the defect distributions.

5. Comparison with experiment

Experimental association energies have been measured for a small number of trivalent impurity ion in MgO. The $MgO:Cr^{3+}$ system was studied by Glass [33] using e.s.r. and optical measurements on annealed samples. He reported values of 0.78 eV and 0.54 eV as lower limit values for the magnitude of the association energies of nn and nnn monomers, respectively. Glass also reported values of 0.32 eV for the magnitude of the additional association energy when a second Cr^{3+} ion is added to a $(Cr_{Mg}V_{Mg})'$ monomer for both dimers A and B. However, due to some assumptions made in the course of the analysis, these results must be regarded as less than reliable [24]. A more recent study on the same system [34] determined a value of 0.88 $\pm$ 0.13 eV for the magnitude of the association energy of a $(Cr_{Mg}V_{Mg})'$ monomer based on diffusion data: it is not clear whether this association energy applies to the nn or nnn monomer or to a combination of these species. The mass-action analysis presented here for the $MgO:Cr^{3+}$ system clearly shows that for lower temperatures and higher impurity concentration, the amount of chromium present in dimeric species may exceed that present in monomeric species. Until recently, experimental evidence existed only for the monomeric species. However, evidence for the existence of dimeric associates has recently been published based on spectroscopic studies of this system [35]. This study identified new lines in the e.s.r. spectra of $MgO:Cr^{3+}$ crystals which were attributed to dimers A and C. A more recent study of the $MgO:Cr^{3+}$ system [36] has identified new lines in the luminescence spectra, which have been attributed to structures in which a third Cr^{3+} ion is located within four to six lattice spacings of dimer A.

The $MgO:Fe^{3+}$ system was investigated by Gourdin *et al.* [37] who studied the oxidation-reduction of iron in MgO and compared their experimental findings with the results of a mass-action analysis of the system. The energies used in this analysis were varied until agreement with experiment was obtained. In this way, they determined values of 0.69 and 0.92 eV for the magnitude of the association energies of nn and nnn $(Fe_{Mg}V_{Mg})'$ monomers, respectively, and 0.56 and 0.46 for the magnitudes of the additional association energies for the formation of dimers A and E, respectively, from the appropriate monomers. However, as the authors point out, these values do not necessarily represent a unique set of parameters for the system. The same system was further investigated by Yager and Kingery [38] using high-temperature e.s.r. spectroscopy to follow the changes in the concentration of nn $(Fe_{Mg}V_{Mg})'$ monomers, as a function of temperature. Interpretation of the results by mass-action analysis yielded a value of 0.85 eV for the magnitude of the association energy of the nn monomer.

The system $MgO:Sc^{3+}$ was investigated by Sempolinski and Kingery [6] using ionic conductivity measurements. As mentioned earlier they obtained a value of 0.73 $\pm$ 0.20 eV for the magnitude of the association energy of a $(Sc_{Mg}V_{Mg})'$ monomer. However, from the type of measurement used, it was not possible to ascertain whether this association energy refers to the nn or nnn monomer.

The agreement with our theoretical values is reasonable for all these systems, but the limited number of impurities for which experimental data are available and the rather large errors inherent in these experimental techniques makes an assessment of the suitability of the potential models used rather difficult. There is, however, one important difference between the theoretical values obtained from the two potentials. Potential II predicts almost the same values for the association energies for a particular defect for impurity ions ranging in size from Co^{3+} (0.060 nm) to Sc^{3+} (0.0745 nm) whereas for Potential I, a definite size dependence is clearly evident. This is due to the

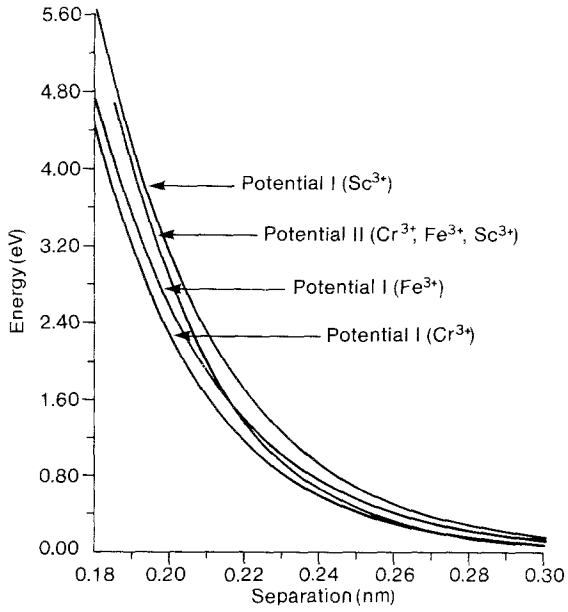

Figure 9 A comparison of the short-range impurity ion–oxygen ion potentials for the ions Cr^{3+}, Fe^{3+} and Sc^{3+} for Potentials I and II.

fact that the short-range impurity–host interactions of Potential II are very similar for all of these ions. Fig. 9 shows the variation in the impurity-oxygen short-range potential with the interionic separation for each of the potentials for the ions Cr^{3+}, Fe^{3+} and Sc^{3+} which have radii of 0.0615, 0.0645 (high spin) and 0.0745 nm, respectively. For our calculations with Potential I, a definite impurity size dependence is evident whereas this is not the case for Potential II. This reflects the way in which these impurity host potentials were derived. Potential I used a fitting procedure incorporating the lattice parameter of the oxide of the impurity ion and thus, indirectly, the impurity ion radius based on oxides. The interactions used in Potential II were derived without recourse to experimental data and therefore might not be expected to correlate to the same extent over a short range of impurity ion sizes. Some correlation is observed, however, for association energies calculated using Potential II over the larger impurity ion radius range, Al^{3+} (0.053 nm) to Y^{3+} (0.090 nm) and is similar to that observed for Potential I.

Little experimental evidence is available for the existence of the kinds of large clusters considered here. There is, however, considerable evidence for the existence of similar clusters and for other different clusters in nonstoichiomeric $Fe_{1-x}O$ which, if regarded as stoichiometric FeO doped with Fe^{3+} ions, is to some extent analogous to the $MgO:M^{3+}$ systems considered here. A study of $Fe_{1-x}O$ [25] was extended to include calculations on the 12–4 cluster proposed by Lebreton and Hobbs [39] which was found to be particularly stable. Experimental evidence for the existence of this cluster had been provided by electron microscopy. The simulation studies concluded that the most stable aggregates resulted from edge sharing rather than corner sharing of the basic 4–1 tetrahedral unit. This contrasts with the present results for $MgO:Fe^{3+}$ systems which favour corner-sharing aggregates.

Experimental evidence for clusters in the $MgO:Fe^{3+}$ system was reported by Waychunas [40] who utilized Mössbauer spectroscopy and EXAFS measurements to estimate the octahedral to tetrahedral (O/T) Fe^{3+} site occupancy ratio. From these measurements, he reported the presence of a range of defect aggregates consisting of basic monomeric and dimeric units and variations about the 4–1 cluster. However, many cluster geometries can be devised with similar O/T ratios and precise determination of the configuration of the clusters present was not possible using these techniques.

The decay of $MgO:Fe^{3+}$ systems supersaturated with monomers was investigated by Yager and Kingery [41] and was found to follow second-order kinetics and to be consistent with the aggregation of a monomer and a dimer to form what is referred to as a 3-cluster, composed of three Fe^{3+} substitutional impurities and two cation vacancies, with an overall effective charge of -1. No specific geometry was proposed for this cluster.

Clearly, in view of the difficulty in determining experimentally the exact structure of larger clusters in these systems, atomistic simulation techniques are particularly useful because they indicate the cluster geometries which are most likely to form. Based on the association energies calculated for the $MgO:Cr^{3+}$ system, using Potential I, the mass action results presented here clearly predict that of the larger clusters considered, only the 4–1(M^{3+}) and the 24–5-a clusters are expected to contribute significantly to the defect equilibria: they would be expected to dominate at lower temperatures.

6. Conclusions

Atomistic simulation techniques have been shown to be extremely useful in the elucidation of the nature and equilibrium distribution of trivalent cationic impurities and their change-compensating vacancies in MgO. These systems have proved difficult to investigate experimentally but the association energies calculated here are in reasonable agreement with the available experimental data. The values of the calculated defect energies depend somewhat on the interionic potential used. The limited experimental information makes it difficult to asses the correctness of these potentials but the semi-empirical potentials were found to reproduce the expected dependence of the association energies on the sizes of the impurity ions rather better than did the potentials derived predominantly from the electron gas approximation.

Incorporation of the theoretical association energies for a range of aggregate defects into a mass-action analysis of the equilibrium distribution of Cr^{3+} ions in MgO predicted that the defect structure would be dominated by dimers and larger clusters at the higher impurity concentrations and at lower temperatures. Of the larger clusters considered, only two, the 4–1(M^{3+}) and 24–5-a were predicted to form in significant concentrations. In general, the calculations show that for clusters based on the 4–1 tetragonal unit those containing M^{3+} interstitial are more stable than those with dipositive host cation interstitials.

Acknowledgements

We are grateful to the Computer Centres at University College Dublin and Trinity College Dublin. JCGC acknowledges the award of a Department of Education Post-graduate Grant.

References

1. M. O. HENRY, J. P. LARKIN and G. F. IMBUSCH, *Phys. Rev. B* **13** (1976) 1893.
2. R. A. WEEKS, J. GASTINEAU and E. SONDER, *Phys. Status Solidi (a)* **61** (1980) 265.
3. J. CORISH, P. W. M. JACOBS and S. RADHAKRISHNA, in "Surface and Defect Properties of Solids", Vol. 6, edited by M. W. Roberts and J. M. Thomas, (The Chemical Society, London, 1977) Ch. 5.
4. B. J. WUENSCH, "Mass Transport Phenomena in Ceramics", edited by A. R. Cooper and A. H. Heuer, Materials Science Research, Vol. 9 (Plenum, New York, 1975) p. 211.
5. R. FREER, *J. Mater. Sci.* **15** (1980) 803.
6. D. R. SEMPOLINSKI and W. D. KINGERY, *J. Amer. Ceram. Soc.* **63** (1980) 664.
7. C. R. A. CATLOW, J. CORISH, K. M. DILLER, P. W. M. JACOBS and M. J. NORGETT, *J. Phys. C.* **12** (1979) 451.
8. P. W. M. JACOBS, J. CORISH and C. R. A. CATLOW, *ibid.* **13** (1980) 1977.
9. J. CORISH, C. R. A. CATLOW, P. W. M. JACOBS and S. H. ONG, *Phys. Rev. B* **25** (1982) 6425.
10. P. J. BENDALL, C. R. A. CATLOW, J. CORISH and P. W. M. JACOBS, *J. Solid State Chem.* **51** (1984) 159.
11. W. H. GOURDIN and W. D. KINGERY, *J. Mater. Sci.* **14** (1979) 2053.
12. E. A. COLBOURN and W. C. MACKRODT, *ibid.* **17** (1982) 3021.
13. M. J. NORGETT, UK AERE Harwell, Report R7650 (1974).
14. C. R. A. CATLOW and W. C. MACKRODT (eds), "Computer Simulation of Solids", in "Lecture Notes in Physics", Vol. 166 (Springer, Berlin, 1982).
15. C. R. A. CATLOW, I. D. FAUX and M. J. NORGETT, *J. Phys. C* **9** (1976) 419.
16. W. C. MACKRODT and R. F. STEWART, *ibid.* **12** (1979) 431.
17. M. J. L. SANGSTER and A. M. STONEHAM, *Phil. Mag. B* **43** (1981) 597.
18. G. V. LEWIS, PhD thesis, University of London (1983).
19. E. A. COLBOURN, J. KENDRICK and W. C. MACKRODT, ICI Corporate Laboratory Report CL-R/81/1637/A (1981).
20. F. A. KROGER and H. J. VINK, *Solid State Phys.* **3** (1956) 307.
21. J. CORISH, J. M. QUIGLEY, P. W. M. JACOBS and C. R. A. CATLOW, *Phil. Mag. A* **44** (1981) 13.
22. P. B. FITZSIMONS and J. CORISH, *Phys. Status Solidi (a)* **91** (1985) 543.
23. A. BRUN and P. DANSAS, *Phys. Status Solidi (b)* **66** (1974) 201.
24. J. C. G. CARROLL, PhD thesis, University of Dublin (1985).
25. C. R. A. CATLOW and B. E. F. FENDER, *J. Phys. C* **8** (1975) 3267.
26. N. L. ALLEN, W. C. MACKRODT and M. LESLIE, *Adv. Ceram.* **23** (1987).
27. G. PECKHAM, *Proc. Phys. Soc.* **90** (1967) 657.
28. G. V. SAMSONOV, "The Oxide Handbook", 2nd Edn (IFI/Plenum, 1982) p. 120.
29. C. R. A. CATLOW, J. CORISH, P. W. M. JACOBS and A. B. LIDIARD, *J. Phys. C* **14** (1981) L121.
30. J. H. HARDING, *Physica* **131B** (1985) 13.
31. N. L. ALLEN and W. C. MACKRODT, unpublished results (1988).
32. S. M. TOMLINSON, C. R. A. CATLOW and J. H. HARDING, UK AERE Harwell, Report TP1095 (1984).
33. A. M. GLASS, *J. Chem Phys.* **46** (1967) 2080.
34. G. W. WEBER, W. R. BITLER and V. S. STUBICAN, *J. Phys. Chem. Solids* **41** (1980) 1355.
35. J. C. G. CARROLL, SARA M. McMURRY, J. CORISH and B. HENDERSON, *J. Phys. C* **18** (1985) 6409.
36. M. B. O NEILL, PhD thesis, University of Strathclyde (1987).
37. W. H. GOURDIN, W. D. KINGERY and J. DRIEAR, *J. Mater. Sci.* **14** (1979) 2074.
38. T. A. YAGER and W. D. KINGERY, *ibid.* **16** (1981) 489.
39. C. LEBRETON and L. W. HOBBS, *Rad. Effects* **74** (1983) 227.
40. G. A. WAYCHUNAS, *J. Mater. Sci.* **18** (1983) 195.
41. T. A. YAGER and W. D. KINGERY, *ibid.* **16** (1981) 483.

Received 19 August
and accepted 1 December 1987